Hydrophobic Interactions in Concentrated Colloidal Suspensions: A Rheological Investigation

Igor Ametov and Clive A. Prestidge*

Ian Wark Research Institute, ARC Special Research Centre for Particle and Material Interfaces, University of South Australia, Mawson Lakes SA 5095, Australia

Received: February 27, 2004; In Final Form: June 10, 2004

Rheological investigations have determined the influence of particle hydrophobicity and solution pH on particle interactions in concentrated suspensions of colloidal silica (advancing water particle contact angles in the range ∼35° to ∼90° have been explored and obtained through surface chemical modification). Suspensions of hydrophilic silica ($\phi = 0.55$) showed negligible viscoelasticity and a pH dependent apparent yield stress. The inverse relationship between the yield stress and the particle ζ-potential squared confirmed that electrical double layer and dispersion forces control particle interactions. On increasing the particle contact angle of silica there is a substantial increase in suspension rheology, i.e., pronounced viscoelasticity and apparent yield stresses, thus suggesting the action of an attractive hydrophobic force. Attempts have been made to deconvolute the various interaction forces, quantify the hydrophobic interaction, and explain the apparent pH dependent non-DLVO behavior.

Introduction

Colloidal interactions between hydrophilic surfaces in aqueous media are commonly described in terms of DLVO theory, which considers only electrical double layer and van der Waals forces. For hydrophobic surfaces (planar or spherical) an attractive, non-DLVO force with a longer range than van der Waals forces has been widely reported.[1−5] The origin of this force has been attributed to the effect of interfacial water structure,[6] patch-wise electrostatic interactions,[7] and cavities or nanobubbles at the interface between hydrophobic surfaces.[8,9] Colloid probe atomic force microscopy (AFM) studies have recently explored the range and magnitude of the forces between hydrophobic colloids and the influence of dissolved gas.[10] Concurrent AFM imaging has shown the existence of nanobubbles on such surfaces;[11,12] their influence on surface forces is considered critical and is the topic of much debate. Hydrophobic interactions in concentrated colloidal suspension, in particular the effect of surface and solution chemistry, have received little quantitative consideration and further investigation is clearly warranted.

Particle interactions in concentrated suspensions are commonly probed with use of rheological methods.[13−26] Scales et al.[24] showed that for particle suspensions where only van der Waals and electrostatic forces are operative, the yield stress (τ_y) can be rationalize

$$\tau_y = K_{struc}\left[\frac{A_H}{12H^2} - \frac{2\pi\epsilon\kappa\zeta^2 e^{-\kappa H}}{1 + e^{-\kappa H}}\right] \quad (1)$$

: where A_H is the Hamaker constant; H is the interparticle distance; $\epsilon = \epsilon_0 D$ with ϵ_0 the permittivity of a vacuum and D the dielectric constant; ζ is the interactive potential well approximated by ζ-potential; κ is inverse Debye length, and K_{struc} is a network structural term dependent on the particle size, solid volume fraction, and the mean coordination number. The terms in the brackets correspond to van der Waals and electrostatic forces, respectively. For suspensions displaying DLVO behavior, eq 1 can be simplified to

$$\tau_y = \tau_{y,max} - k_y\zeta^2 \quad (2)$$

where $\tau_{y,max}$ is the maximum value of the yield stress, which occurs at the isoelectric point (IEP) of the particles, and k_y is a constant. Many suspension rheology studies have confirmed that the yield stress scales linearly with the particle ζ-potential squared.[16−22] This approach has been extended to account for additional interactions to those from electrostatic and dispersion forces, by the addition of a non-DLVO contribution to the yield stress (τ'_y):[22]

$$\tau_y = \tau_{y,max} - k_y\zeta^2 + \tau'_y \quad (3)$$

τ'_y has been shown to be positive in sign and contribute significantly to the overall yield stress for suspensions of kaolinite,[16] poly(methyl methacrylate) and polystyrene latexes,[17] sphalerite,[19,20] galena,[21,22] and surfactant coated zirconia,[26] where hydrophobic attractive forces are in action. In contrast, τ'_y has been shown to be negative for gibbsite suspensions[22] at pH values greater than the IEP. Under similar conditions, AFM has revealed a repulsive interaction force between gibbsite particles and this is considered to be due to either hydration or a steric layer at the particle surface.[27,28]

For hydrophobic particle systems, the pull-off (adhesion) force determined by colloid probe AFM has been correlated with the suspension yield stress.[20,26] For hydrophobic ZrO_2 colloids, Leong et al.[26] showed that the yield stress correlated with the hydrophobic and van der Waals forces rather than electrostatic forces, even at pH values away from the IEP. For ZnS particles, Muster et al.[20] showed a positive correlation between the adhesion force and the yield stress, but demonstrated that the surface chemistry is critical for sulfide particles and can be influenced by the surface area-to-volume ratio. These studies

* Address correspondence to this author. E-mail: clive.prestidge@unisa.edu.au.

10.1021/jp0491257 CCC: $27.50
Published on Web 07/21/2004

did not fully explore the interplay between particle hydrophobicity, solution conditions, yield stress, and interaction forces.

In this study we investigate the influence of surface modification and solution chemistry on the rheological behavior of concentrated silica particle suspensions. In particular, the influence of particle hydrophobicity (controlled by TMCS treatment and characterized in terms of a particle contact angle) and ζ-potential (controlled by pH) on the rheology and particle interaction behavior is investigated. The magnitude of DLVO and non-DLVO forces in controlling the particle interaction behavior is elucidated.

Experimental Section

Materials and Suspension Preparation. Silica spheres were obtained from Geltech Inc. (Alachua, FL). According to the manufacturer specification the particle density was 2.0 g cm^{-3}. Scanning electron microscopy showed the particles to be highly monodispersed with a diameter of 0.6 $\pm$ 0.05 μm. Gas adsorption and BET analysis showed a specific surface area of 3.9 $\pm$ 0.1 m^2 g^{-1} and confirmed nonporosity. On the basis of the equivalent spherical diameter, laser diffraction gave a specific surface area of 4.1 m^2 g^{-1}, again confirming the low level of porosity.

Trimethylchlorosilane (TMCS) (Aldrich, USA) and cyclohexane (L.R. grade, Aldrich, USA) were distilled prior to use. High-purity water was produced by a Milli-Q purification system. All other reagents were analytical grade. All silica suspensions were prepared in a 10^{-3} M KNO_3 background electrolyte. The suspension pH was controlled by small additions of potassium hydroxide or nitric acid solutions.

The surface chemistry of silica particles was modified by treatment with TMCS. Hydrated silica was first heated at 130 °C for 15 h to remove surface moisture then treated for 1 h in a shaken reaction vessel with solutions of TMCS in cyclohexane (10^{-2} and 5×10^{-3} M). The silica particles were then washed with cyclohexane, dried in a clean oven at 50 °C, and stored in a vacuum desiccator prior to characterization, suspension preparation, and rheological analysis.

Suspensions were prepared by adding known weights of silica particles to known volumes of electrolyte solution at pH 8 and stirring the solution for 15 h with a magnetic stirrer. Suspension volume fractions were checked from the dry weight. Dynamic light scattering and laser diffraction were used to confirm that the silica particle samples were fully dispersed at mildly alkaline conditions.

Methods. *Particle Contact Angles.* Contact angles of silica particles were determined from the rate of penetration into a particle-packed capillary, i.e., the Washburn approach.[29−31] A consistently packed bed of particles is essential and was achieved by using the following procedure. A known weight of silica particles was tapped into a capillary tube plugged at one end with a 4−5 mm section of glass wool to retain particles. The capillaries were then vibrated until a powder volume fraction of ~0.6 was obtained. The height of the liquid rise was then measured as a function of time. The advancing water contact angle was evaluated from

$$\cos\theta_p = \frac{(h^2/t)_p \eta_p \gamma_w}{(h^2/t)_w \eta_w \gamma_p} \quad (4)$$

where h is the height of a liquid rise through a packed bed after a time t, and γ and η are the wetting liquid surface tension and viscosity. Partially and completely wetting liquids are denoted by p and w, respectively. Cyclohexane was previously shown to be a perfectly wetting liquid for glass beads coated with hydroxypropyl methylcellulose[30] and was, therefore, chosen for the current studies. Advancing water contact angles of particles were determined with errors of $\pm$3%.

Electrokinetic Properties. ζ-potentials of silica particles were calculated from electrophoretic mobility data obtained with use of phase analysis light scattering (PALS). The electrophoretic mobility was determined from the amplitude-weighted phase difference as an average of five runs and converted to ζ-potential by using the Smoluchowski equation ($\kappa a \gg 1$).

Rheological Properties. Rheological measurements in both static and dynamic modes were conducted with use of a Rheometrics SR-5000 stress-controlled rheometer with parallel plate sample geometry (40-mm diameter and 1.5-mm gap). The sample temperature was controlled to 25 $\pm$ 0.1 °C with a Peltier element and digital temperature control bath. For flow curve measurements the applied stress was increased linearly from 0.1 N m^{-2} to 200 N m^{-2} and the deformation determined; viscosity versus shear stress (or shear rate) curves were then obtained. For dynamic measurements the elastic (G') and viscous moduli (G'') were determined as a function of applied stress at an oscillation frequency of 1 Hz (G' and G'' are linked by the phase angle (δ), i.e., $\tan\delta = G''/G'$). Direct yield stress measurements were made by using the vane technique,[25] i.e., from the maximum in a stress (or torque) versus time curve, using a vane tool and a Haake VT550 rheometer operating at 0.1 rpm. The extrapolated (or Bingham) yield stress, τ_B, was determined by linear extrapolation of shear stress versus shear rate curves to zero shear rate.

Results and Discussion

Surface Chemistry, Wettability, and Electrokinetics. Three levels of silica particle surface modification have been investigated: (A) hydrated silica particles, without methylation and with a particle contact angle of 30 $\pm$ 5°; (B) methylated silica (0.005 M TMCS) with a particle contact angle of 80 $\pm$ 3°; and (C) methylated silica (0.01 M TMCS) with a particle contact angle of ~90°

Sample A has a fully hydroxylated surface and is considered hydrophilic. The small, but finite, contact angle is in good agreement with reports on similar colloidal silica particles.[32] In contrast, single surfaces and multi-micron sized silica or quartz particles have zero contact angles.[33,34] It should be noted that the high surface energy of colloidal silica makes them susceptible to surface contamination and conspires to induce measurement difficulties when measuring contact angles on dry particles (e.g. the Washburn approach). The intermediate contact angle of sample B confirms partial methylation. Sample C is extensively methylated by TMCS and the advancing water contact angle of ~90° is in good agreement with reported contact angles for methylated quartz particles[35] and single surfaces.[36−38] Blake and Ralston[35] have suggested that a fully methylated quartz surface, with contact angle of ~90°, corresponds to a surface coverage by methyl groups of 0.72 $\pm$ 0.09. On the basis of a Cassie[39] approach we predict sample B to have a surface coverage of methyl groups of 0.62. Samples B and C may well display surface chemical heterogeneities, i.e., hydrophobic and hydrophilic patches.[40] It should be noted that no significant contact angle variation was detected and the contact angles of samples B and C are stable after treatment in aqueous solution for 24 h.

ζ-potential versus pH plots for the silica particle samples are presented in Figure 1; these measurements were undertaken by decreasing the pH from 8 down to 3, i.e., in the same manner

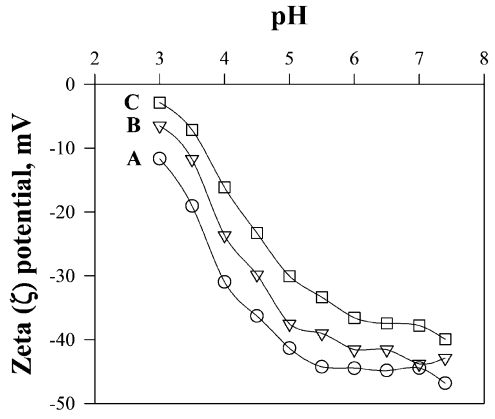

Figure 1. ζ-potential of silica particles in 0.001 M KNO_3 background electrolyte as a function of pH and particle hydrophobicity (A, $\theta = 30°$; B, $\theta = 80°$; C, $\theta \approx 90°$) measured with PALS.

that rheological measurements were made. Interestingly, we have shown that equivalent ζ-potential values measured from low to high pH are significantly lower in magnitude and those with a different pH dependency. These differences are considered to be due to the surface chemical changes (e.g. hydration levels, formation of polymeric structures, and formation of surface nanobubbles) that may occur at low pH and cause variations in the electrical double layer properties.

It is clear from Figure 1 that as the level of surface chemical modification and hydrophobicity increases, the magnitude of the ζ-potential significantly decreases. The general shape of the ζ-potential versus pH curves and the IEP values (in the range pH 2.5 to 3) are independent of surface chemical modification. A number of previous studies[35,41,42] have reported that the ζ-potentials of silica or quartz particles are independent of methylation. However, others have reported ζ-potential variation with surface methylation and this is clearly an area of some debate. It has been suggested that upon methylation of the silica surface, trimethylsilyl groups replace only 2.6 of the total 4.6 silanols per nm^2 and that this is not sufficient to change the ζ-potential. According to Healy and Grieser,[43] the number of silanol groups on the surface should be reduced below 0.5 per nm^2 for significant changes of the ζ-potential.

More recently, Churaev et al.[40] reported that the ζ-potential of methylated quartz capillaries, measured through streaming potential, decreases in magnitude over a period of time in contact with electrolyte solutions. They attributed this to the progressive formation of nanoscopic gas bubbles on the methylated surface from the flowing electrolyte solution. Upon a sharp increase in the electrolyte flow rate, the ζ-potential reverted to its original value, presumably due to the partial detachment of these gas bubbles. No such effect was observed for nonmethylated and "bubble free" methylated surfaces. Snoswell et al.[44] studied the influence of silica particle hydrophobicity and solution concentration of CO_2 on particle ζ-potential. At higher than equilibrium concentration of CO_2 (10^{-2} M) the ζ-potential of methylated particles was lower in comparison with that of clean, hydrophilic particles. With this in mind, it may be hypothesized that the ζ-potential versus pH variation that we observe with increasing levels of methylation results from adsorbed nanobubbles that shift the shear plane away from the surface. Even though surface ionization mechanisms for surface charging are considered to be dominant, we also acknowledge that ion adsorption phenomena that play an important role in determining the surface charge and ζ-potential behavior of gas bubbles[45] and oil droplets[46] may also influence the ζ-potential of the hydrophobic silica samples.

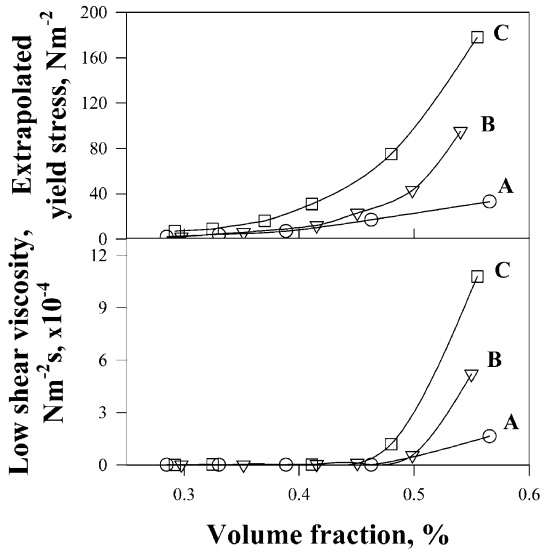

Figure 2. Extrapolated yield stress and low shear viscosity of silica suspensions (0.001 M KNO_3 background electrolyte, pH 3) as a function of solids volume fraction and particle hydrophobicity (A, $\theta = 30°$; B, $\theta = 80°$; C, $\theta \approx 90°$).

Suspension Rheology. *General Rheological Behavior.* The rheology of silica suspensions is strongly dependent on the particle volume fraction, the particle surface chemistry, and the solution conditions. In this study we are primarily interested in the influence of solution pH and particle hydrophobicity, but first a suitable particle volume fraction is required to enable these variables to be explored with high sensitivity. Figure 2 shows the influence of particle volume fraction on the low shear viscosity and the extrapolated yield stress of the silica particle samples; these measurements were undertaken at pH 3, i.e., near the IEP where repulsive electrostatic forces are minimal and the rheological parameters are maximized. Away from the IEP (e.g. at pH 7) the rheological parameters are considerably reduced; this effect is explored in the following sections. The rheological parameters become significant at particle volume fractions (ϕ) greater than 0.5 and are more pronounced for the more hydrophobic particles; again this is explored further below. A ϕ value of 0.55 was selected for further study.

Viscosity versus shear stress plots for silica particle suspensions ($\phi = 0.55$) over the pH range of 3 to 8 are presented in Figure 3. Irrespective of surface modification, the suspensions exhibit shear thinning behavior and, as the pH is decreased, become more extensively shear thinning and show a substantial increase in their low shear viscosity. The magnitude of the low shear viscosity and the degree of shear thinning is greater for the more hydrophobic silica samples. In a similar manner the viscoelastic properties of the silica suspensions are strongly dependent on the pH and hydrophobicity, see Figure 4 and Table 1. The extent of a suspension's linear viscoelastic region (i.e. stress range where G' is independent of stress) and magnitude of moduli values decrease significantly with pH; this effect is most pronounced for the more hydrophobic particles. Sample A displays negligible viscoelasticity at greater than pH 5, with G' and G'' values in the 10^2 to 10^3 N m^{-2} range at pH <5. Samples B and C exhibit G' and G'' values in the ranges 10^3 to 10^4 and 10^4 to 10^5 N m^{-2}, respectively. Furthermore, sample C displays linear viscoelastic behavior over a wider pH range and more extensive elastic structure ($\tan\delta = G''/G'$ is in the range 0.2−0.3 for sample C, whereas $\tan\delta \sim 1$ for samples A and B). Evidence of yield stresses can also be observed in both the static and dynamic rheological data and will be discussed in the following section.

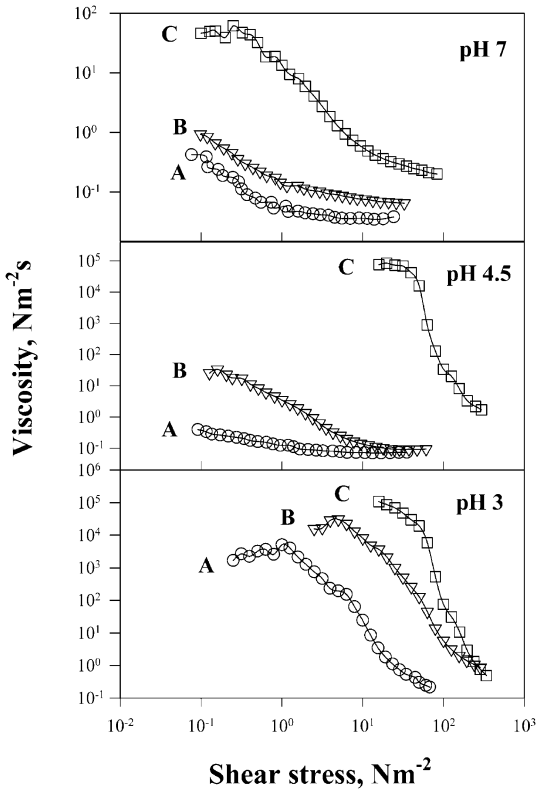

Figure 3. Viscosity vs shear stress data for silica suspensions in 0.001 M KNO_3 background electrolyte as a function of pH and particle hydrophobicity (A, $\theta = 30°$; B, $\theta = 80°$; C, $\theta \approx 90°$).

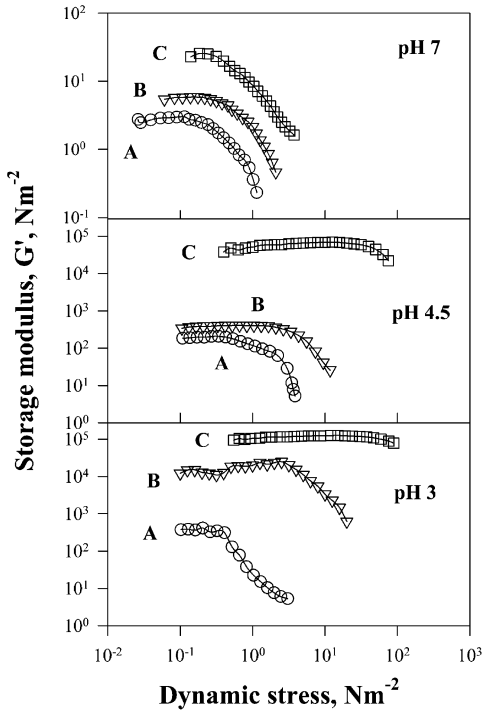

Figure 4. Storage modulus vs dynamic stress data for silica suspensions in 0.001 M KNO_3 background electrolyte as a function of pH and particle hydrophobicity (A, $\theta = 30°$; B, $\theta = 80°$; C, $\theta \approx 90°$).

For any particular silica suspension sample, as the pH is reduced the rheological parameters increase; this behavior can be reconciled in terms of the reduced ζ-potential (see Figure 1) and subsequently weaker electrostatic forces, i.e., as expected for DLVO behavior. The observed increase in rheological parameters as the silica particle contact angle is increased, and the pH influence on this effect, is considered to be due to the introduction of additional hydrophobic forces of an attractive nature.

TABLE 1: Dynamic Data for Silica Suspensions of $\phi = 0.55$ in 0.001 M KNO_3 Background Electrolyte at Particle Contact Angles (θ) of 30°, 80°, and 90°

	$\theta \approx 30°$		$\theta \approx 80°$		$\theta \approx 90°$	
pH	G', N m^{-2}	G'', N m^{-2}	G', N m^{-2}	G'', N m^{-2}	G', N m^{-2}	G'', N m^{-2}
3.0	360	300	18500	19000	125000	35000
3.5	680	480	16800	17000	121000	31000
3.75	470	400	8500	7700		
4.0	670	510				
4.5	190[a]	110[a]	380	110	59000	20000
5.0	4[a]	3[a]	8[a]	3[a]		
5.5	1	1			3400	670
6.0					280	70
7.0	1	1			23[a]	21[a]
8.0					6[a]	9[a]

[a] No linear viscoelastic region observed.

Yield Stresses and the Influence of Solution and Surface Chemistry. Though there is much debate over the precise meaning of a "yield stress", the yield stress is the rheological parameter that has been most extensively used to relate suspension rheology and particle interaction behavior. For the silica suspensions under investigation there is clear evidence from both static (Figure 3) and dynamic (Figure 4) rheological data that a critical (yield) stress is observed at the onset of flow. In practical terms the vane method[25] is the preferred approach for reliable τ_y determination and this has been used in the current investigation. A vane yield stress investigation with a range of vane sizes and a range of vane rotation rates showed that τ_y values were in the range 0.01 and 1 N m^{-2} for silica suspensions at $\phi = 0.55$. However, the measurements were highly variable and insensitive toward subtle changes in surface and solution chemistry. Comparable investigations on concentrated alumina[24] and zirconia[47] suspensions reported τ_y values within the 100−1500 N m^{-2} range. This difference is due to the substantially lower Hamaker constant (A_H) of silica (0.83×10^{-20} J) than alumina (5.2×10^{-20} J) or zirconia (8.8×10^{-20} J) and hence the reduced van der Waals interactions. Also silica particle surfaces have an additional repulsive nature due to "hydration forces"[48−50] that have been attributed to a "sterically stabilizing gel layer" of polymeric silicates formed by solubilization and readsorption at the silica surface.[50,51] With these thoughts in mind, the extrapolated (or Bingham) yield stress, τ_B, determined by linear extrapolation of shear stress versus shear rate curves to zero shear rates was used. The extrapolated yield stress proved to be more discriminatory in the context of the present investigation (it is, however, recognized that τ_B represents some equilibrium position between an attractive particle networks being pulled apart and is generally an over-estimation of the classically defined yield stress). Of further note, the critical stress from either static (viscosity versus shear stress data) or dynamic (storage modulus versus oscillatory stress data) measurement was also used to estimate τ_y. Both τ_y and τ_B are used in the following discussion.

Yield stress data for the silica suspensions are plotted as a function of pH in Figure 5. Irrespective of silica particle surface chemistry, τ_y and τ_B increase with decreasing pH and reach maximum values near the IEP, where repulsive forces are minimized and attractive forces dominate. As the hydrophobicity of the silica particles is increased the suspensions exhibit significantly higher yield stress values, indicating the presence of an attractive force. In a similar manner, Leong et al.[47]

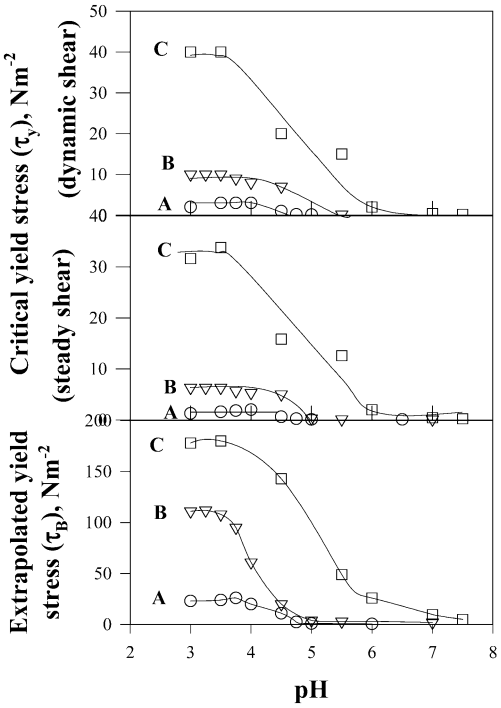

Figure 5. Extrapolated and critical yield stress for silica suspensions in 0.001 M KNO_3 background electrolyte as a function of pH and particle hydrophobicity (A, $\theta = 30°$; B, $\theta = 80°$; C, $\theta \approx 90°$).

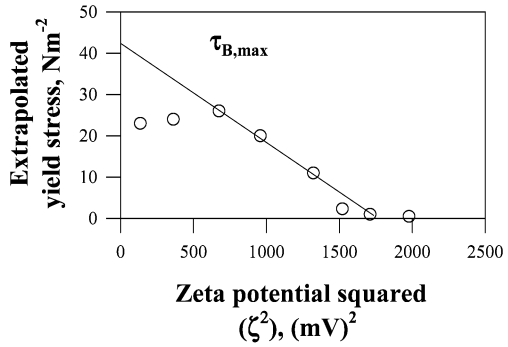

Figure 6. Extrapolated yield stress for the suspension of hydrophilic silica in 0.001 M KNO_3 background electrolyte as a function of ζ-potential squared.

observed a sharp rise in τ_y for zirconia suspensions hydrophobised with anionic surfactant.

Hydrophobicity and Particle Interactions. On consideration of eqs 1, 2, and 3 and in an attempt to further reconcile particle interaction forces in silica particle suspensions, it is instructive to plot yield stress values as a function of ζ-potential squared.

Suspensions of Hydrophilic Silica. For suspensions of hydrophilic silica (sample A) the yield stress decreases linearly with increasing ζ-potential squared over the range 750 to 1600 $(mV)^2$, i.e., eq 2 is followed and electrostatic forces control particle interaction (DLVO behavior), see Figure 6. At ζ-potential magnitudes less than ~25 mV, i.e., at pH values near the IEP, the yield stress is lower than would be predicted by only DLVO forces (eq 2). "Hydration" forces are known to act between silica surfaces and have been directly measured;[52] these are considered to be responsible for the observed deviation from DLVO behavior. By assuming DLVO behavior at ζ-potential magnitudes greater than ~25 mV, the yield stress data follows eq 3 and can be described by

$$\tau_y = \tau_{y,max} - k_y\zeta^2 + \tau'_y \qquad (3)$$

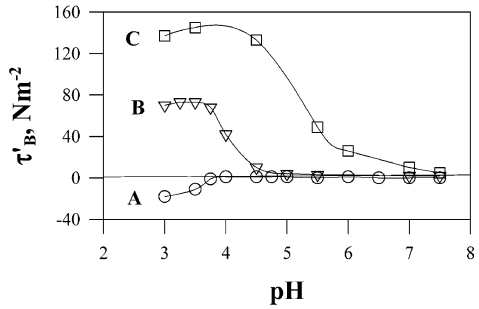

Figure 7. Non-DLVO component τ'_B for silica suspensions in 0.001 M KNO_3 background electrolyte as a function of pH and particle hydrophobicity (A, $\theta = 30°$; B, $\theta = 80°$; C, $\theta \approx 90°$).

TABLE 2: Parameters of Eq 2 (from steady and dynamic stress data), and Non-DLVO Component of Eqs 3 and 5 at pH 3 for Silica Particle Suspensions

	sample		
parameter	A	B	C
$\tau_{y,max}$, N m^{-2} (steady stress data)	3	7	32
k_y (steady stress data)	0.002	0.004	0.02
$\tau'_{y,pH3}$, N m^{-2} (steady stress data)	−2	+3	+28
$\tau'_{y,max}$, N m^{-2} (dynamic stress data)	5	11	39
k_y (dynamic stress data)	0.0027	0.0052	0.026
$\tau'_{y,pH3}$, N m^{-2} (dynamic stress data)	−4	+4	+34
$\tau_{B,max}$, N m^{-2}	45	113	188
k_B	0.03	0.08	0.12
$\tau'_{B,pH3}$, N m^{-2}	−18	+68	+134

and similarly for the extrapolated yield stress

$$\tau_B = \tau_{B,max} - k_B\zeta^2 + \tau'_B \qquad (5)$$

Values of τ'_y and τ'_B for sample A are pH dependent and negative at pH below 4 (plotted in Figure 7), i.e., the additional non-DLVO component is of a repulsive nature. The findings confirm that hydration forces are short-ranged and only influence the particle interaction potential near the IEP, where electrostatic forces are negligible.

Suspensions of Hydrophobic Silica. On consideration of eq 1, let us assume the following: K_{struc}, and hence k_y and k_B in eqs 3 and 5, are equivalent for samples A, B, and C (i.e. the number of particle contacts in the aggregated suspension is constant), A_H (i.e. magnitude of van der Waals forces) is independent of the silica sample surface chemistry, and $\tau_{y,max}$ obtained for hydrophilic silica suspensions (sample A) determines the magnitude of van der Waals interactions.

Then eqs 3 and 5 may be applied to the yield stress data for hydrophobic silica particles (samples B and C). In this case, τ'_y and τ'_B are positive in magnitude, increase significantly with the hydrophobicity, and are pH dependent (see Figure 7 and Table 2). Although a number of theories have been proposed to explain hydrophobic interactions, the "bubbles on the surface" theory has recently received considerable experimental support. AFM imaging[11,12] demonstrated that surface hydrophobicity and roughness play an essential role in the formation of small bubbles at a solid−water interface. Theoretical analysis by Mishchuk et al.[53] based on only DLVO forces demonstrated that the presence of small bubbles on the surface of a particle leads to an attraction similar to that often described as a hydrophobic force. Furthermore, they showed that the attraction between the particle and a macrobubble increases with increasing bubble surface coverage and their diameters. Thus, we speculate that small bubbles form on the surface of methylated silica particles of samples B and C changing the nature of particle interactions. Of further note, sample C, being more

hydrophobic may have either bubbles of larger diameters on particle surfaces or greater bubble surface coverage.

We now address the pH dependence of the additional silica particle interactions introduced due to hydrophobicity. In systems open to the atmosphere, dissolved gas will inevitably be present in the aqueous phase. Carbon dioxide has the highest solubility in water compared with other atmospheric gases, and has been reported to enhance hydrophobic interactions.[10,44,54,55] A component of dissolved CO_2 is hydrated, forming carbonic acid, whereas the remainder is present as individual molecules and/or very small bubbles. At high pH, [HCO_3^-] species prevail in solution, and nucleation of bubbles on the particle surfaces is less likely. Indeed, τ'_y and τ'_B are insignificant for samples B and C at pH >7. Dai et al.[54] proposed that HCO_3^- ions are adsorbed more strongly on hydrophobic particles than OH^-, hence when the pH decreases the formation of carbon dioxide takes place near the surface of the particles, resulting in a low level of local supersaturation, which can trigger bubble nucleation. This is in accord with the work of Ryan and Hemmingsen,[56] who showed that bubble nucleation at hydrophobic and porous surfaces does not require high levels of gas supersaturation. We hypothesize that the increase in τ'_y and τ'_B with decreasing pH for samples B and C originates from microbubbles forming and/or growing on the surface of hydrophobic particles driven by local CO_2 supersaturation. The number of bubble nucleation sites and the size of grown bubbles determine the magnitude of τ'_y and τ'_B for samples B and C, and is related to the particle hydrophobicity.[12]

For the particles with small bubbles protruding from the surface, in the absence of electrical double layer interactions (e.g. close to the i.e.p.), the total interaction energy will be determined by a combination of particle−water−particle, bubble−water−particle, and bubble−water−bubble interactions.[44] Upon bubble coalescence the additional interactions will occur, namely the interaction of silica particles across a gaseous phase, we presume CO_2, and capillary forces due to CO_2 bridging the two particles. Notably, the mentioned contributions are van der Waals interactions with the bubble−water−particle interaction being negative in sign.[53] On the basis of Hamaker constant values, bubble−water−bubble and particle−CO_2−particle interactions would dominate and their magnitude would increase with increased bubble coverage and particle hydrophobicity. The bubble−water−bubble and particle−CO_2−particle interactions would also determine the magnitude of $\tau_{y,max}$ and $\tau_{B,max}$ (eq 2). On the basis of eq 2 the yield stress for suspensions B and C is plotted as a function of ζ- potential squared (see Figure 8). For both samples, the yield stress decreases linearly with increasing ζ^2. The values of k_y, k_B, $\tau_{y,max}$, and $\tau_{B,max}$ for samples A, B, and C (presented in Table 2) increase significantly with increased particle contact angle. Interestingly, eq 2 is followed over the range 0 to 1600 $(mV)^2$ indicating the absence of non-DLVO repulsive forces. Methylation with TMCS changes the surface chemistry of silica particles and is most likely responsible for the nonappearance of a "hydration" force. On the other hand, if present, "hydration" forces would only become detectable at separation distances <2 nm, which are unachievable when 20−60 nm bubbles[12] protrude from the surfaces. The increase in k_y and k_B with particle hydrophobicity (see Table 2) is likely related to changes in floc structure. Suspensions of hydrophilic silica (sample A) would have flocs with open structure, i.e., with a low average number of contacts per particle or coordination number. Such suspensions generally do not show high yield stresses. For sample B, small gas bubbles present on the surface may result in an increased number of particle contacts, hence enhanced aggregation levels and higher yield stresses. For sample C, with the highest contact angle, due to a potentially increased nanobubble surface coverage a continuous particle network may form; this would be reflected in substantially higher yield stress of the suspensions and is in agreement with the observations.

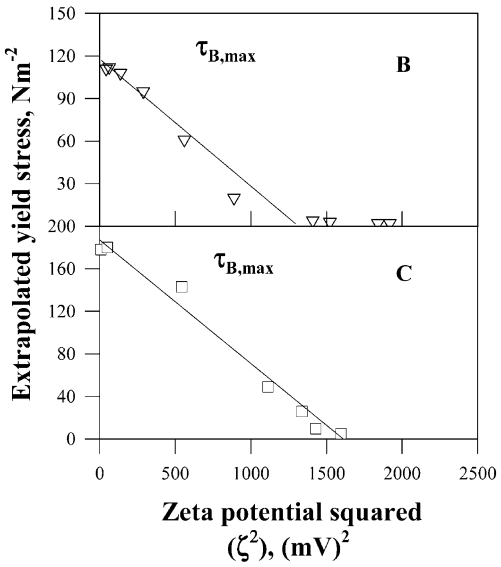

Figure 8. Extrapolated yield stress as a function of ζ-potential squared for the silica suspensions (samples B and C) in 0.001 M KNO_3 background electrolyte.

Conclusions

Rheological investigations have been successfully used to probe the nature of hydrophobic interactions in concentrated suspensions of chemically modified silica particles. At pH values away from the IEP, particle interactions in suspensions of hydrophilic silica can be described by using DLVO theory, i.e., the suspension yield stress scales linearly with ζ-potential squared. At pH values near the IEP the yield stress shows a negative deviation from the DLVO theory; this is presumed due to repulsive "hydration" forces. Rheological investigations of hydrophobic silica suspensions reveal a significant attractive force and hence increased yield stresses; this influence increases with particle contact angle and is more pronounced at low pH. A plausible explanation is that the additional attractive force originates from the changes in magnitude of van der Waals forces due to interactions between the small bubbles protruding from the surface of hydrophobic particles.

References and Notes

(1) Israelashvili, J. N.; Pashley, R. M. *Nature* **1982**, *300*, 341.
(2) Pashley, R. M.; McGuiggan, P. M.; Ninham, B. W.; Evans, D. F. *Science* **1985**, *229*, 1088.
(3) Claesson, P. M.; Christenson H. K. *J. Phys. Chem.* **1988**, *92*, 1650.
(4) Rabinovich, Y. I.; Derjaguin, B. V. *Colloids Surf.* **1988**, *30*, 243.
(5) Parker, J. L.; Claesson, P. M. *Langmuir* **1994**, *10*, 635.
(6) Eriksson, J. C.; Ljunggren, S.; Claesson, P. M. *J. Chem Soc. Faraday Trans.* **1989**, *285*, 162.
(7) Ruckenstein, E.; Churaev, N. V. *J. Colloid Interface Sci.* **1991**, *147*, 535.
(8) Christenson, H. K.; Claesson, P. M. *Science* **1988**, *239*, 390.
(9) Meagher, L.; Craig, V. S. J. *Langmuir* **1994**, *10*, 2736.
(10) Manke, J.; Stearnes, J.; Hayes, R. A.; Fornasiero, D.; Ralston, J. *Phys. Chem. Chem. Phys.* **1999**, *1*, 2793.
(11) Tyrrell, J. W. G.; Attard, P. *Langmuir* **2002**, *18*, 160.
(12) Yang, J. W.; Duan, J. M.; Fornasiero, D.; Ralston, J. *J. Phys. Chem.* **2003**, *107*, 6139.
(13) Leong, Y. K.; Boger, D. V. *J. Rheol.* (*N.Y.*) **1990**, *35*, 149.

(14) Leong, Y. K.; Boger, D. V.; Scales, P. J.; Healy, T. W.; Buscall, R. *J. Chem. Soc. Chem. Commun.* **1993**, *7*, 639.
(15) Heath, D.; Tadros, Th. F. *J. Colloid Interface Sci*. **1983**, *93*, 307.
(16) Hunter, R. J.; Nicole, S. K. *J. Colloid Interface Sci*. **1968**, *28*, 250.
(17) Friend, J. P.; Hunter, R. J. *J. Colloid Interface Sci*. **1971**, *37*, 548.
(18) Hunter, R. J. *Adv. Colloid Interface Sci.* **1982**, *17*, 197.
(19) Muster, T. H.; Prestidge, C. A. *Miner. Eng.* **1995**, *8*, 1541.
(20) Muster, T. H.; Toikka, G.; Hayes, R. A.; Prestidge, C. A.; Ralston, J. *Colloids Surf.* **1996**, *106*, 203.
(21) Prestidge, C. A. *Colloids Surf.* **1997**, *126*, 75.
(22) Prestidge, C. A. *Min. Pro. Ext. Met. Rev*. **1999**, *20*, 57.
(23) Prestidge, C. A.; Ametov, I.; Addai-Mensah, J. *Colloids Surf. A* **1999**, *157*, 137.
(24) Scales, P. J.; Johnson, S. B.; Healy, T. W.; Kapur, P. C. *AIChE J.* **1998**, *44*, 538.
(25) Nguyen, Q. D.; Boger, D. V. *J. Rheol.* (*N.Y.*) **1983**, *27*, 321.
(26) Leong, Y. K.; Boger, D. V.; Scales, P. J.; Healy, T. W. *J. Colloid Interface Sci*. **1996**, *181*, 605.
(27) Addai-Mensah, J.; Dawe, J.; Hayes, R. A.; Prestidge, C. A.; Ralston, J. *J. Colloid Interface Sci*. **1998**, *203*, 115.
(28) Addai-Mensah, J.; Prestidge, C. A.; Ralston, J. *Miner. Eng.* **1999**, *12*, 655.
(29) Washburn, E. W. *Phys. Rev.* **1921**, *17*, 273.
(30) Parsons, G. E.; Buckton, G.; Chatham, S. M. *Int. J. Pharm.* **1992**, *82*, 145.
(31) Yang, Y. W.; Zografi, G.; Miller, E. E. *J. Colloid Interface Sci.* **1988**, *122*, 35.
(32) Muster, T. H.; Prestidge, C. A.; Hayes, R. A. *Colloids Surf. A* **2001**, *176*, 253.
(33) Scales, P. J.; Grieser, F.; Furlong, D. N.; Healy, T. W. *Colloids Surf. A* **1986**, *21*, 55.
(34) Subrahmanyam, T. V.; Monte, M. B. M.; Middea, A.; Valdiviezo, E.; Lins, F. F. *Miner. Eng.* **1999**, *12*, 1347.
(35) Blake, P.; Ralston, J. *Colloids Surf.* **1985**, *15*, 101.
(36) Lamb, R. M.; Furlong, D. N. *J. Chem. Faraday Trans.* **1982**, *78*, 1, 61.
(37) Pashley, R.; Kitchener, J. A. *J. Colloid Interface Sci.* **1979**, *71*, 491.
(38) Xu, Z.; Yoon, R.-H. *J. Colloid Interface Sci.* **1990**, *134*, 427.
(39) Cassie, A. B. D. *Discuss. Faraday Soc.* **1948**, *3*, 11.
(40) Churaev, N. V.; Ralston, J.; Sergeeva, I. P.; Sobolev, V. D. *Adv. Colloid Interface Sci.* **2002**, *96*, 265.
(41) Laskowski, J.; Kitchener, J. A. *J. Colloid Interface Sci.* **1969**, *29*, 670.
(42) Harding, R. D. *J. Colloid Interface Sci.* **1971**, *35*, 172.
(43) Healy, T. W.; Grieser, F. Division of Colloid and Surface Chemistry, RACI 7th National Convention, Canberra, August, 1972.
(44) Snoswell, D. R. E.; Duan, J.; Fornasiero, D.; Ralston, J. *J. Phys. Chem. B* **2003**, *107*, 2986.
(45) Graciaa, A.; Morel, G.; Saulnier, P.; Lachaise, J.; Schechter, R. S. *J. Colloid Interface Sci.* **1995**, *172*, 131.
(46) Marinova, K. G.; Alargova, N. D.; Denkov, N. D.; Velev, O. D.; Petsev, D. N.; Ivanov, I. B.; Borwankar, R. P. *Langmuir* **1996**, *12*, 2045.
(47) Leong, Y. K.; Boger, D. V.; Scales, P. J.; Healy, T. W. *J. Colloid Interface Sci*. **1996**, *181*, 605.
(48) Healy, T. W. In *The Colloid Chemistry of Silica*; ACS Advances in Chemistry Ser. No. 234; Bergna, H. E., Ed.; American Chemical Society: Washington, DC, 1994; Chapter 7.
(49) Vigil, G.; Xu, Z.; Stainberg, S.; Israelachvili, J. N. *J. Colloid Interface Sci.* **1994**, *165*, 367.
(50) Yates, D. E.; Healy, T. W. *J. Colloid Interface Sci*. **1976**, *55*, 9.
(51) Tadros, Th. F.; Lyklema, J. *Electroanal. Chem. Interfacial Electrochem*. **1968**, *17*, 267.
(52) Chapel, J.-P. *Langmuir* **1994**, *10*, 4237.
(53) Mishchuk, N.; Ralston, J.; Fornasiero, D. *J. Phys. Chem. A* **2002**, *106*, 689.
(54) Dai, Z.; Fornasiero, D.; Ralston, J. *J. Chem. Soc., Faraday Trans.* **1998**, *94*, 1983.
(55) Gong, W.; Stearnes, J.; Fornasiero, D.; Hayes, R. A.; Ralston, J. *Phys. Chem. Chem. Phys.* **1999**, *1*, 2799.
(56) Ryan, W. L.; Hammingsen, E. A. *J. Colloid Interface Sci.* **1998**, *197*, 101.